Proc. Natl. Acad. Sci. USA
Vol. 92, pp. 10506–10510, November 1995
Chemistry

Calicheamicin–DNA complexes: Warhead alignment and saccharide recognition of the minor groove

NORIHIRO IKEMOTO*, R. AJAY KUMAR*, TAO-TAO LING*, GEORGE A. ELLESTAD†, SAMUEL J. DANISHEFSKY‡, AND DINSHAW J. PATEL*§

*Cellular Biochemistry and Biophysics Program and ‡Molecular Pharmacology and Experimental Therapeutics Program, Memorial Sloan–Kettering Cancer Center, New York, NY 10021; and †Wyeth-Ayerst Research, Pearl River, NY 10965

Contributed by Samuel J. Danishefsky, July 25, 1995

ABSTRACT **The solution structures of calicheamicin γ_1^I, its cycloaromatized analog (calicheamicin ε), and its aryl tetrasaccharide complexed to a common DNA hairpin duplex have been determined by NMR and distance-refined molecular dynamics computations. Sequence specificity is associated with carbohydrate–DNA recognition that places the aryl tetrasaccharide component of all three ligands in similar orientations in the minor groove at the d(T-C-C-T)·d(A-G-G-A) segment. The complementary fit of the ligands and the DNA minor groove binding site creates numerous van der Waals contacts as well as hydrogen bonding interactions. Notable are the iodine and sulfur atoms of calicheamicin that hydrogen bond with the exposed amino proton of the 5′- and 3′-guanines, respectively, of the d(A-G-G-A) segment. The sequence-specific carbohydrate binding orients the enediyne aglycone of calicheamicin γ_1^I such that its C^3 and C^6 proradical centers are adjacent to the cleavage sites. While the enediyne aglycone of calicheamicin γ_1^I is tilted relative to the helix axis and spans the minor groove, the cycloaromatized aglycone is aligned approximately parallel to the helix axis in the respective complexes. Specific localized conformational perturbations in the DNA have been identified from imino proton complexation shifts and changes in specific sugar pucker patterns on complex formation. The helical parameters for the carbohydrate binding site are comparable with corresponding values in B-DNA fibers while a widening of the groove is observed at the adjacent aglycone binding site.**

Calicheamicin γ_1^I (**1**, Fig. 1) has received considerable interest from the organic chemistry community because of its architecture, important bioactivity, and intriguing mechanism of action (1). It is a very potent tumoricidal agent that functions by efficiently cutting DNA. This is carried out by the enediyne aglycone functionality (the "warhead") of calicheamicin upon progression to a highly reactive diradical species that abstracts hydrogens from the DNA sugar backbone. Calicheamicin γ_1^I targets oligopyrimidine-oligopurine tracts with a preference for the d(T-C-C-T)·d(A-G-G-A) sequence (2–5). The binding specificity has been attributed to the long aryl tetrasaccharide segment of calicheamicin γ_1^I (6). This sector, as its methyl glycoside (**2**, Fig. 1), has been shown to competitively inhibit DNA cleavage by calicheamicin γ_1^I (7, 8) as well as suppress binding of a protein transcription factor to its preferred d(T-C-C-T)·d(A-G-G-A)-containing DNA binding site (9). An improved understanding of the contributions of the diverse array of novel functional groups in the carbohydrate recognition domain should provide a foundation for the design of the next generation of carbohydrate-based DNA binding drugs. The aryl tetrasaccharide component also has an important role in properly anchoring the warhead for sequence-selective double strand cleavage, since the aglycone by itself primarily generates random single strand cuts in the DNA (7).

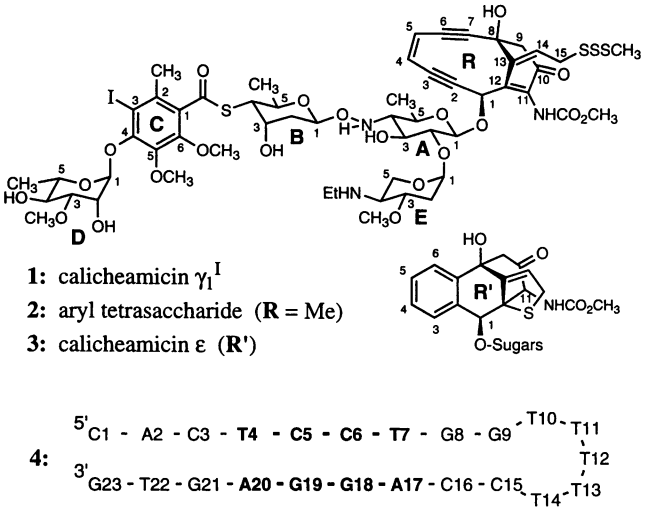

FIG. 1. Ligand structures and DNA sequence used for structural studies.

We report below on a combined NMR/molecular dynamics approach toward determination of a distance-refined solution structure of calicheamicin γ_1^I **1** bound to DNA hairpin duplex **4** containing the central d(T-C-C-T)·d(A-G-G-A) segment. Previous NMR structural studies on calicheamicin–DNA oligomer complexes were guided by a few intermolecular nuclear Overhauser effects (NOEs) (≈15 restraints) between the drug and the DNA with the emphasis on the nonexchangeable proton data (10, 11). By contrast, our ability to identify and assign a larger number of intermolecular NOEs (≈70 restraints) using exchangeable and nonexchangeable proton data in the calicheamicin γ_1^I–DNA hairpin duplex complex has permitted extension of the structural efforts to higher resolution. The resulting distance-refined structures have provided insights into the contributions of individual interactions between the drug and the DNA to the observed sequence specificity and cleavage chemistry.

In addition to the calicheamicin γ_1^I–DNA complex, we have conducted parallel structural studies with the aryl tetrasaccharide domain **2** and the cycloaromatized analog, calicheamicin ε (**3**, Fig. 1) bound to the same DNA hairpin duplex **4**. Such comparative structural studies should define whether the carbohydrate components of **1**, **2**, and **3** bind to the same site on DNA hairpin duplex **4** and, in addition, provide insights into the orientation of the enediyne-based diradical species during the DNA cleavage process.

The publication costs of this article were defrayed in part by page charge payment. This article must therefore be hereby marked "*advertisement*" in accordance with 18 U.S.C. §1734 solely to indicate this fact.

Abbreviations: NOE, nuclear Overhauser effect; NOESY, NOE spectroscopy; COSY, correlated spectroscopy; TOCSY, total correlated spectroscopy.

§To whom reprint requests should be addressed.

MATERIALS AND METHODS

Preparation of the Complexes. The drugs in methanol (d_4) were titrated into a solution of DNA hairpin duplex **4** (250 ODs for the aryl tetrasaccharide, 480 ODs for calicheamicin γ_1^I, and 450 ODs for calicheamicin ε) in pH 7 NMR buffer solution (100 mM NaCl/10 mM sodium phosphate/0.1 mM EDTA). The proton resonances of the free DNA hairpin duplex and the drug–DNA complexes were in slow exchange with imino proton markers utilized to monitor formation of the one drug per duplex complexes. The samples were lyophilized to remove the methanol and dissolved in aqueous buffer.

NMR Experiments. All NMR experiments were performed on Varian Unity Plus 500- and 600-MHz NMR spectrometers. Proton assignments in the complexes were made following analysis of NOE spectroscopy (NOESY) data sets in ^2H_2O buffer at 10°C, 20°C, and 30°C in conjunction with ^{1}H-COSY45, TOCSY, and ^{1}H–^{31}P COSY data sets (where COSY is correlated spectroscopy and TOCSY is total correlated spectroscopy) at 20°C, and ^{1}H–^{13}C HMQC data sets at 30°C. The NOESY buildup data on the complex in ^2H_2O buffer were acquired at 10°C with mixing times of 40, 80, 120, and 160 ms and with a relaxation delay of 5 s for the calicheamicin γ_1^I complex and 3 s for calicheamicin ε and aryl tetrasaccharide complexes. The NOESY spectra in H_2O buffer were acquired using the WATERGATE pulse sequence (12) at 5°C, with a 60-ms mixing time and a 1.5-s relaxation delay. The NMR data were processed using the VNMR software (Varian) and the NOE cross peaks were integrated using the XEASY software (13).

Distance and Torsional Restraints. The interproton distances were estimated from the buildup of NOE intensities as a function of mixing time. A quadratic polynomial was fitted to the data points and the initial slope was calculated from the linear fit of the quadratic curves to the first non-zero mixing time. The cytidine H5 to H6 distance of 2.48 Å was used as the standard for interproton distances. The upper and lower bounds were assigned to each distance based on the residuals of the fit between the buildup data and the quadratic polynomials. The dihedral angles for the deoxyribose sugars of the DNA and the pyranose sugars of the drugs were calculated from the patterns of COSY45 cross peaks. Simulation of the cross peaks using the CHORDS program (14) provided the coupling constants, which were converted to dihedral angle restraints using a modified Karplus equation. The ε torsional angle restraints were estimated from the H3′–P coupling constants, which were obtained from the H3′-selective ^{1}H–^{31}P COSY experiment (15).

Molecular Dynamics Calculations. The starting structure was constructed using the parameters for a B-form DNA, and the drug in an extended conformation was placed >6 Å outside the minor groove. The T_5 loop was not included in the structure calculations. The initial model and parameters for calicheamicin were generated using the program QUANTA (v3.3, Molecular Simulations, Waltham, MA) and converted to X-PLOR format. A total charge of +1.0 was assigned to the drug because sugar E has a protonated ethylamino group. The starting structures were subjected to 500 steps of conjugate gradient minimization. Restrained molecular dynamics with simulated annealing was carried out in vacuum with full charges and a distance-dependent dielectric constant using the program X-PLOR (16). All distance restraints were imposed in the form of square-well potentials. The dynamics was initiated at 5 K, and the temperature was gradually increased to 1000 K in 5.0 ps and then equilibrated for 1.0 ps. The force constants for the distance restraints were kept at 2.0 kcal·mol^{-1}·Å^{-2} (1 kcal = 4.18 kJ) during these stages. Subsequently, the force constants for the distance restraints were scaled up to a final value of 30 kcal·mol^{-1}·Å^{-2} over 6.0 ps. The system was then allowed to evolve for 10.0 ps at 1000 K before slow cooling to 300 K in 7.0 ps and was then equilibrated for another 10.0 ps. The coordinates saved every 0.5 ps for the last 4.0 ps were averaged, and the resulting structure was minimized. All dynamics were carried out with a time step of 0.5 fs, and the force constant on the Watson–Crick hydrogen bond-related distance restraints were maintained at 60.0 kcal·mol^{-1}·Å^{-2} throughout.

RESULTS AND DISCUSSION

NMR Spectra and Assignments. The imino proton spectral region (12.4–14.4 ppm) of the free DNA hairpin duplex **4** (Fig. 2*A*) and the one drug per duplex complexes with calicheamicin γ_1^I **1** (Fig. 2*B*), calicheamicin ε **3** (Fig. 2*C*), and the aryl tetrasaccharide **2** (Fig. 2*D*) exhibit well-resolved resonances consistent with formation of a predominant single conformation of the complex in each case.

The through space and through bond analysis of the two-dimensional data sets in H_2O and ^2H_2O solution has yielded a near complete list of exchangeable and nonexchangeable proton chemical shifts of the drugs and the DNA in the three complexes. This has in turn permitted us to identify the intermolecular NOEs that define the relative alignment of the drugs in the DNA minor groove for the three complexes.

Solution Structures of Complexes. The protocol for the distance restrained molecular dynamics calculations are outlined in *Materials and Methods.* Eight structures were calculated for each complex using random number seeds for the initial velocities with the calculations guided by the distance and torsion angle restraints. The intermolecular drug–DNA NOE distributions for each of the complexes are outlined in Table 1. A larger number of intermolecular NOEs are detected from the drugs to the d(A-G-G-A)-containing strand relative to the d(T-C-C-T)-containing strand in all three complexes

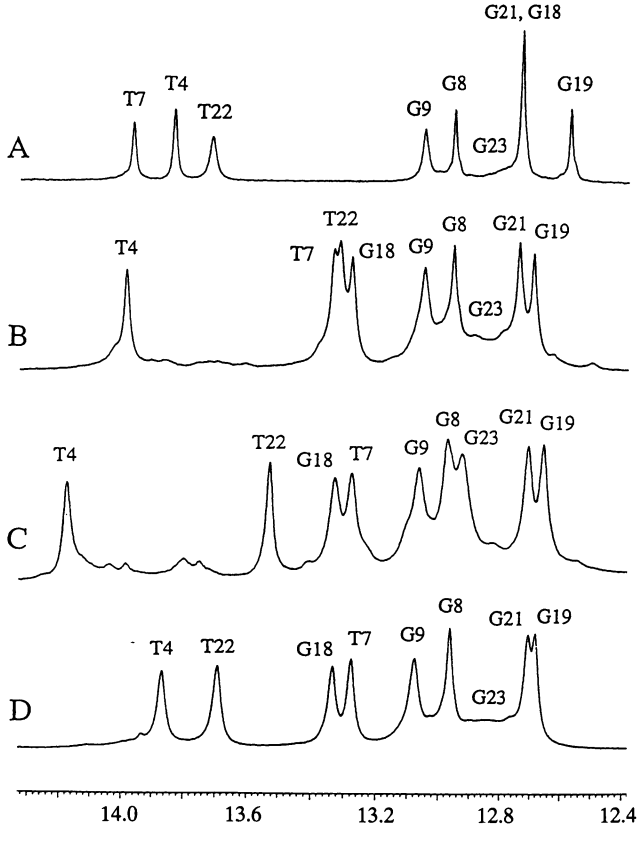

FIG. 2. Imino proton NMR spectra (12.4–14.3 ppm) for the free DNA hairpin duplex **4** (*A*) and its complexes (one drug per duplex) with calicheamicin γ_1^I (*B*), calicheamicin ε (*C*), and aryl tetrasaccharide (*D*) in H_2O buffer (pH 7) at 25°C.

Table 1. Intermolecular drug–DNA NOEs for the DNA hairpin duplex **4** complexed with calicheamicin γ_1^I **1**, aryl tetrasaccharide **2**, and calicheamicin ε **3**, subdivided by drug residues and DNA (containing TCCT and AGGA) strands

	Cal. γ_1^I **1**		Saccharide **2**		Cal. ε **3**	
	TCCT	AGGA	TCCT	AGGA	TCCT	AGGA
R	1	4	—	—	7	6
A	0	6	2	4	0	4
B	8	10	8	6	5	4
C	5	13	4	9	2	7
D	6	14	3	13	0	12
E	3	0	4	0	2	0
	23	47	21	32	16	33
Total	70		53		49	

Cal., calicheamicin.

(Table 1). The calicheamicin γ_1^I–DNA complex structure calculations were based on 70 intermolecular drug–DNA restraints with the resulting eight structures (Fig. 3) exhibiting a root mean square deviation (rmsd) with standard deviation of 0.94 ± 0.17 Å (excluding terminal base pairs). The corresponding eight structures for the calicheamicin ε–DNA and aryl tetrasaccharide–DNA complexes exhibited rmsd values of 1.39 ± 0.29 Å and 1.18 ± 0.18 Å, respectively (excluding terminal base pairs). Representative structures of calicheamicin γ_1^I **1**, calicheamicin ε **3**, and aryl tetrasaccharide **2** complexes with the DNA hairpin duplex **4** are shown in color in Fig. 4 *B*, *C*, and *A*, respectively.

The drugs bind in the minor groove with the complexes exhibiting a common carbohydrate binding site, which spans the d(T4-C5-C6-T7)·d(A17-G18-G19-A20) segment of the duplex (Fig. 4). The carbohydrate segments adopt a fully extended conformation with the matching complementarity between the surfaces of the drug and the DNA minor groove excluding water molecules from this intermolecular interface.

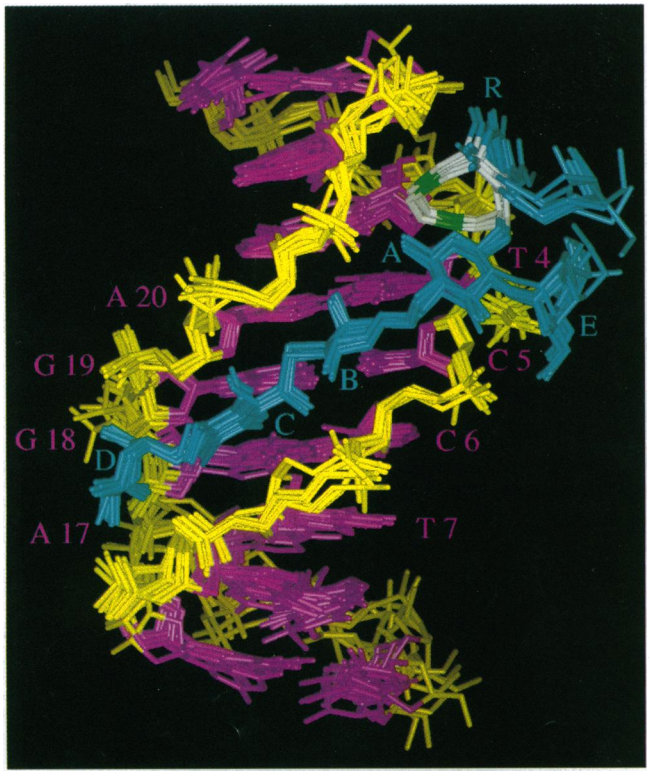

FIG. 3. Eight superposed distance-refined solution structures of the calicheamicin γ_1^I–DNA hairpin duplex complex. The DNA bases and backbones are colored in magenta and yellow, respectively, with labeling of the residues in the d(T4-C5-C6-T7)·d(A17-G18-G19-A20) segment. The drug is colored in cyan with the enediyne-containing ring in white and the C^3 and C^6 pro-radical centers in green. The calicheamicin γ_1^I residues are also labeled (R, A, B, C, D, and E rings).

Carbohydrate–DNA Recognition. The B-C unit of the aryl tetrasaccharide segment occupies the center of the d(T-C-C-T)·d(A-G-G-A) minor groove binding site and exhibits extensive base-specific contacts with the DNA in all three complexes. The thio sugar B is positioned edgewise in the minor groove and contacts the A20 residue through van der Waals and hydrogen bonding (B ring hydroxyl to N^3 of the base) interactions. The aromatic ring C is positioned between the walls of the minor groove with its iodine and CH_3 groups directed toward the floor of the minor groove. These edge-on orientations of rings B and C deep in the minor groove are defined by the intermolecular NOE patterns [strong cross peak between B(H3) and A20(H2); cross peaks between the CH_3 protons of ring C and the imino and exposed amino protons of G18 and G19] and the large shielding of the minor groove H4′ protons of T7 and A20 (Table 2) that are positioned directly over the opposite faces of the aromatic ring C. The S-carbonyl linker, which adopts an orthogonal alignment relative to the plane of ring C (favored by the steric demands of the *ortho* aromatic ring substituents), bridges the minor groove and makes van der Waals contacts with the opposing walls of the groove.

Schreiber and colleagues (17) have proposed a stabilizing interaction (based on modeling studies) between the iodine atoms on ring C of calicheamicin γ_1^I and the exocyclic amino groups of the guanines in the d(A-G-G-A)·d(T-C-C-T) segment of the DNA duplex. Subsequent experiments have established that iodine is critical for binding to this segment since the binding affinity for complex formation reduces in the order I > Br > Cl > F > CH_3 > H (18). Further, the amino group of the 5′-guanine in the d(A-G-G-A) segment is a critical recognition element since its replacement by inosine (lacking a 2-amino group) results in a greatly reduced binding to calicheamicin γ_1^I (18). These constraints are met in our solution structures of the complexes that show direct DNA-to-ligand hydrogen bonding interaction between the exposed amino proton of G18 and the iodine atom of calicheamicin. In addition, the sulfur atom of the S-carbonyl linker connecting rings B and C forms an intermolecular hydrogen bond with the exposed amino proton of G19. This latter interaction was also observed in the solution structure of the esperamicin A_1–DNA complex (19). Juxtaposition of these large, polarizable iodine and sulfur atoms of calicheamicin against the floor of the minor groove induces large chemical shift changes, resulting in an ≈4 ppm chemical shift difference between the geminal amino protons for G18 and G19 in the d(A-G-G-A) binding site segment (Table 2).

The amino sugar A is aligned face down over T4 of the oligopyrimidine strand and is anchored by a potential intermolecular hydrogen bond between its hydroxyl group and the backbone phosphate at the C5–C6 step in the drug–DNA complexes. The orthogonal alignment of the adjacent A and B sugars is achieved through an eclipsed conformation at the unusual NH-O linkage (10, 11, 19) in all three complexes. The rhamnose sugar D penetrates less deeply into the minor groove and its alignment is defined, in part, by intermolecular hydrogen bonds between its hydroxyl groups (OH-2 and OH-4) and the backbone phosphates (G19-A20 and G8-G9 steps, respectively) in the complex. The E sugar straddles the sugar-phosphate backbone at the d(C3-T4-C5) segment with its positively charged ethylamino group interacting with the backbone phosphate at the C3–T4 step.

Aglycone Alignment. The C^2-C^3-C^4-C^5-C^6-C^7 enediyne segment of the aglycone effector region of calicheamicin γ_1^I is positioned deep in the minor groove with its cyclic ring system bridging the sugar-phosphate backbone on partner strands.

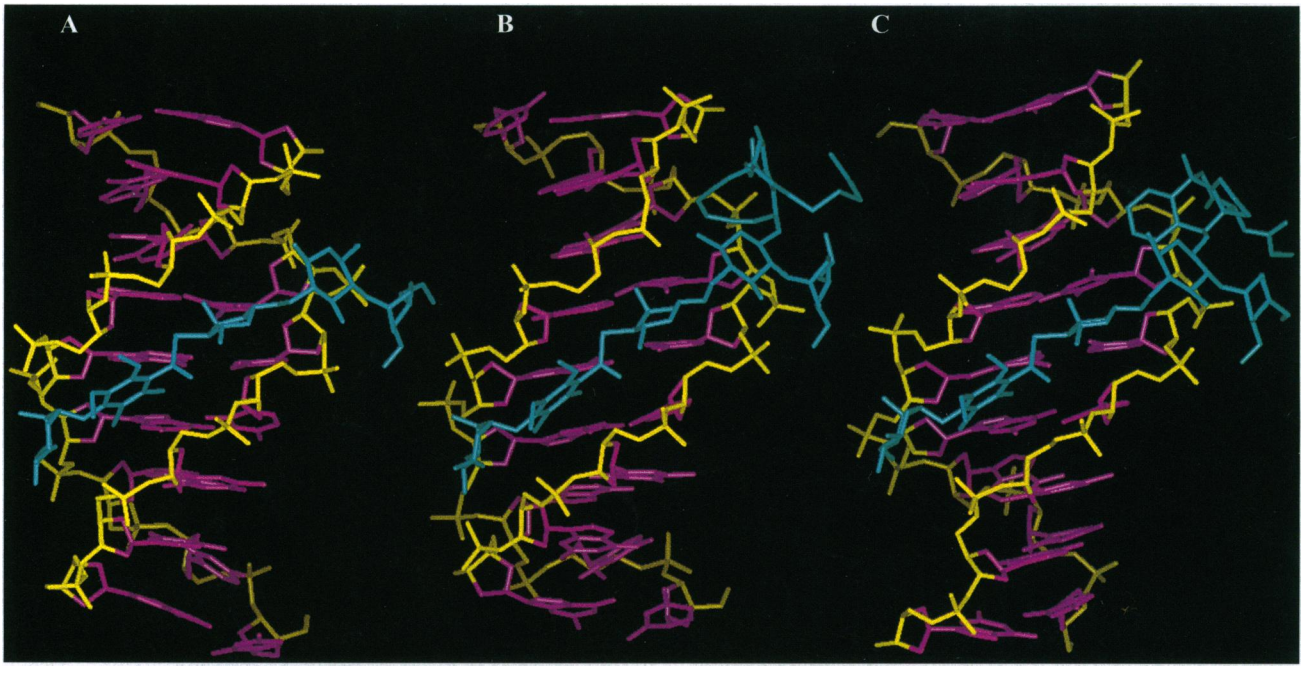

FIG. 4. Representative distance-refined solution structures for the DNA hairpin duplex **4** complexed with aryl tetrasaccharide (*A*), calicheamicin γ_1^I (*B*), and calicheamicin ε (*C*).

The intermolecular NOE patterns involving the enediyne H4 (δ = 6.08 ppm) and H5 (δ = 6.24 ppm) protons [cross peaks H4 to T4(H1′) and H5 to T22(H1′)] position them in the floor of the minor groove with the warhead spanning the groove in the complex. This alignment is anchored by a potential hydrogen bond between the hydroxyl group of C^8 on the enediyne ring and the backbone phosphate at the T22-G23 step in the complex.

Our attempts to replace the C3·G21 base pair that flanks the d(T-C-C-T)·d(A-G-G-A) segment by other base pair combinations (C·I, I·C, and A·T pairs) resulted in calicheamicin γ_1^I forming a heterogeneous mixture of two or more complexes (resulting in a reduction in the fraction of the primary binding site) on the DNA hairpin duplex **4**.

Calicheamicin γ_1^I cleaves both strands of duplex DNA by abstracting hydrogens from partner strands (3, 20, 21) that correspond to the H5′ (pro S) of C5 and H4′ of T22 in our DNA hairpin duplex **4**. The C^3 and C^6 pro-radical centers of the enediyne ring are proximal to their expected abstraction sites since we measure average separations of 2.98 Å (C^3 to H5′ of C5) and 3.22 Å (C^6 to H4′ of T22) in our solution structure of the calicheamicin γ_1^I–DNA hairpin duplex **4** complex.

Table 2. Proton chemical shifts (ppm) for the DNA resonances of the three drug–DNA complexes that exhibit large complexation shifts

	Cal γ_1^I **1**	Saccharide **2**	Cal. ε **3**
Imino			
T7	13.35 (−0.77)	13.29 (−0.83)	13.25 (−0.87)
G18	13.41 (+0.61)	13.36 (+0.56)	13.31 (+0.51)
Amino			
G18	9.10, 4.34*	9.04, 4.29	9.03, 4.28
G19	8.28, 3.68	8.17, 3.66	8.27, 3.59
H4′			
T7	2.40 (−1.70)	2.37 (−1.72)	2.39 (−1.71)
A20	3.25 (−1.17)	3.19 (−1.24)	3.16 (−1.27)

Upfield and downfield complexation shifts in parentheses are defined by − and + signs, respectively. Cal., calicheamicin.
*Hydrogen-bonded amino protons are downfield from their exposed counterparts.

The cycloaromatized aglycone ring of calicheamicin ε **3** is aligned approximately parallel to the helix axis in its complex with the DNA hairpin duplex **4** (Fig. 4*C*). This may reflect the extra steric demand introduced by the H3 and H6 cycloaromatized ring protons in the calicheamicin ε–DNA complex. The change in the hybridization at C^{11} reorients the carbamate side chain to point the carbonyl away from the groove in the calicheamicin ε–DNA complex, which contrasts with the horizontal orientation in the calicheamicin γ_1^I–DNA complex.

Conformational Perturbations on Complex Formation. There has been considerable interest in the nature of potential structural perturbations in the DNA associated with binding of calicheamicin γ_1^I to the d(T-C-C-T)·d(A-G-G-A) site on the helix. Calicheamicin γ_1^I **1**, calicheamicin ε **3**, and the aryl tetrasaccharide **2** bind to the DNA hairpin duplex **4** with retention of all A·T and G·C base pairs in a Watson–Crick alignment on complex formation. The width of the minor groove (measured as the shortest H4′-H4′ separation across the groove) covers the range 5.8 ± 0.4 Å with an *x* displacement of +0.1 ± 0.4 Å for the central segment of the calicheamicin γ_1^I–DNA hairpin duplex complex. These values can be compared with the corresponding parameters in B-DNA (width = 5.8 Å and *x* displacement = −0.7 Å) and A-DNA (width = 12.5 Å and *x* displacement = −5.4 Å). The minor groove width widens to 7.9 ± 0.2 Å at the enediyne binding site [C5(H4′)-T22(H4′) separation] in order to accommodate the aglycone in the calicheamicin γ_1^I–DNA complex.

A quantitative analysis of conformational transitions associated with complex formation would require the solution structures of the free drug and free DNA in aqueous solution, which are currently unavailable. However, there are qualitative indications of local conformational perturbations in the DNA helix associated with changes in NMR parameters (chemical shifts and coupling constants) on complex formation. Thus, the imino proton of T7 shifts upfield while the imino proton of G18 shifts downfield within the d(T4-C5-C6-T7)·d(A17-G18-G19-A20) segment in all three complexes (Table 2 and Fig. 2). Such shifts would most likely require alterations in the relative stacking of adjacent C6·G18 and T7·A17 base pairs on complex formation. Further, the imino proton of T22 at the aglycone binding site of the DNA hairpin duplex **4** shifts upfield on

formation of the calicheamicin γ_1^I **1** and calicheamicin ε **3** complexes but not the aryl tetrasaccharide **2** complex. All nonterminal sugar puckers in the stem of the free DNA hairpin duplex **4** adopt C2′-*endo* sugar puckers in solution. By contrast, the C6 sugar at the carbohydrate binding site adopts an O4′-*endo* pucker in all three complexes while the T22 sugar at the aglycone binding site adopts an O4′-*endo* pucker only for the calicheamicin γ_1^I and calicheamicin ε complexes. Finally, we detect broad cross peaks (10, 11) in the two-dimensional spectra associated with proton resonances of residue C5 in all three complexes that were not detected for the free DNA hairpin duplex. These perturbations identify base pair overlaps and sugar puckers that appear to participate in localized DNA conformational changes associated with calicheamicin–DNA complex formation.

Summary. The carbohydrate segment of calicheamicin γ_1^I constitutes the crucial recognition element for targeting the d(T-C-C-T)·d(A-G-G-A) sequence. This carbohydrate framework displays a diverse array of functional groups that form extensive hydrogen bonding and van der Waals contacts with the DNA minor groove to stabilize the complex, and optimal complementarity of fit is achieved through localized conformational changes in the DNA. With the carbohydrate thus bound, the attached aglycone is properly directed into the minor groove for sequence-specific double strand cleavage. Our structural studies of these interactions have provided an improved understanding of how calicheamicin achieves its remarkable binding selectivity and set the stage for design of additional carbohydrate-based DNA targeting agents.

R.A.K. is a postdoctoral fellow of the Miriam and Benedict Wolf Cancer Research Fund.

1. Nicolaou, K. C. & Dai, W.-M. (1991) *Angew. Chem. Int. Ed. Engl.* **30,** 1387–1416.
2. Zein, N., Sinha, A. M., McGahren, W. J. & Ellestad, G. A. (1988) *Science* **240,** 1198–1201.
3. Zein, N., Poncin, M., Nilakantan, R. & Ellestad, G. A. (1989) *Science* **244,** 697–699.
4. Walker, S., Landovitz, R., Ding, W. D., Ellestad, G. A. & Kahne, D. (1992) *Proc. Natl. Acad. Sci. USA* **89,** 4608–4612.
5. Mah, S. C., Townsend, C. A. & Tullius, T. D. (1994) *Biochemistry* **33,** 614–621.
6. Drak, J., Iwasawa, N., Danishefsky, S. J. & Crothers, D. M. (1991) *Proc. Natl. Acad. Sci. USA* **88,** 7464–7468.
7. Aiyar, J., Danishefsky, S. J. & Crothers, D. M. (1992) *J. Am. Chem. Soc.* **114,** 7552–7554.
8. Nicolaou, K. C., Tsay, S.-C., Suzuki, T. & Joyce, G. F. (1992) *J. Am. Chem. Soc.* **114,** 7555–7557.
9. Ho, S. N., Boyer, S. H., Schreiber, S. L., Danishefsky, S. J. & Crabtree, G. R. (1994) *Proc. Natl. Acad. Sci. USA* **91,** 9203–9207.
10. Walker, S., Murnick, J. & Kahne, D. (1993) *J. Am. Chem. Soc.* **115,** 7954–7961.
11. Paloma, L. G., Smith, J. A., Chazin, W. J. & Nicolaou, K. C. (1994) *J. Am. Chem. Soc.* **116,** 3697–3708.
12. Piotto, M., Sandek, V. & Sklenar, V. (1992) *J. Biomol. NMR* **2,** 661–665.
13. Xia, T.-H., Bartels, C. & Wuthrich, K. (1993) XEASY, ETH Automated Spectroscopy for X Window Systems, User Manual (ETH, Honggerberg, Zurich).
14. Majumdar, A. & Hosur, R. V. (1992) *Prog. Nucl. Magn. Reson. Spectrosc.* **24,** 109–158.
15. Sklenar, V. & Bax, A. (1987) *J. Am. Chem. Soc.* **109,** 7525–7526.
16. Brünger, A. T. (1993) X-PLOR, A System for X-Ray Crystallography and NMR (Yale Univ., New Haven, CT), Version 3.1.
17. Hawley, R. C., Kiessling, L. L. & Schreiber, S. L. (1989) *Proc. Natl. Acad. Sci. USA* **86,** 1105–1109.
18. Li, T., Zeng, Z., Estevez, V. A., Baldenius, K. U., Nicolaou, K. C. & Joyce, G. F. (1994) *J. Am. Chem. Soc.* **116,** 3709–3715.
19. Ikemoto, N., Kumar, R. A., Dedon, P. C., Danishefsky, S. J. & Patel, D. J. (1994) *J. Am. Chem. Soc.* **116,** 9387–9388.
20. Hangeland, J. J., De Voss, J. J., Heath, J. A., Townsend, C. A., Ding, W. D., Ashcroft, J. S. & Ellestad, G. A. (1992) *J. Am. Chem. Soc.* **114,** 9200–9202.
21. Dedon, P. C., Salzberg, A. A. & Xu, J. (1993) *Biochemistry* **32,** 3617–3622.